Design and Torque-Mode Control of a Cable-Driven Rotary Series Elastic Actuator for Subject-Robot Interaction*

Junkai Lu[1], Kevin Haninger[1], Wenjie Chen[2], and Masayoshi Tomizuka[1]

Abstract— To achieve a compact, lightweight and compliant actuator design for intrinsically safe subject-robot interactions, a Bowden cable-driven rotary series elastic actuator is proposed in this paper. To realize the zero output torque control of the proposed actuator in the presence of variable friction of the Bowden cable, a disturbance observer based torque-mode control algorithm is developed and analyzed. The effectiveness of the proposed design is verified by experiments with a human subject.

I. INTRODUCTION

Subject-robot interactions become more and more common in today's society, in fields such as factory automation, rehabilitation, and service. The subject could be other robots, humans, or even animals, and thus the need to ensure the subjects' safety requires the robot actuation mechanism to be able to operate in an ideal force/torque-mode control with intrinsic compliance. The series elastic actuator (SEA) proposed in [1] can serve as a simple but effective solution due to its possession of an elastic component between the motor and the load/subject.

Rotary SEAs (RSEA) have been widely used in applications where direct contact occurs between the subject and the robot, and typical applications are in upper/lower extremity exoskeleton designs. Most RSEAs impose the motor on the subject body [2]–[5] using gears as the power transmission mechanism, which reduces the system compactness and also increases the inertia of the overall system. To achieve a lightweight and compact design, [6] proposes a Bowden cable-driven RSEA which is able to avoid attaching the motors on the subject body. In such an architecture, the geared motor can be installed on a fixed base and the driving force is transmitted through the Bowden cable to the subject body segment. One challenge with this design is to account for the variable friction of the Bowden cable. A sensor fusion approach is proposed in [6] to compensate such friction using two sets of RSEAs with ten sensors.

In order to reduce the hardware cost and complexity of the cable-driven RSEA for a single joint, a simpler design approach is proposed in this paper. The background of this work is to provide the actuation of an elbow joint exoskeleton which is to be worn by the macaques in a brain-machine interface (BMI) study conducted at UC Berkeley. At the

current stage, it is required that the actuator should be able to track the natural motion of the subject's elbow ideally with zero output impedance. To deal with the friction of the Bowden cable, a disturbance observer (DOB) based torque-mode control algorithm is developed due to its nice properties of being able to robustly reject the disturbance as well as to reshape the plant model [2], [7], [8].

Another challenge arises from the treatment of the subject motion in the system model. [2] introduces an assumed relationship between the angles of the subject joint and the actuator joint, and thus the plant to be controlled is coupled with both the subject and the motor model. In this paper, we first separate the actuator loop and the subject loop to design the torque-mode controller by treating the subject motion as an exogenous reference to the actuator loop, and then the stability of the overall actuator-subject system is analyzed together with the designed torque-mode controller.

This paper is organized as follows: the mechanical design of the proposed cable-driven RSEA is described in Section II; the system modeling and torque-mode controller design is discussed in Section III; the designed control algorithm is implemented and evaluated in Section IV. Section V concludes this paper and proposes some future work.

II. MECHANICAL DESIGN OF CABLE-DRIVEN RSEA

Fig. 1 shows the hardware setup of the proposed cable-driven RSEA. The joint side mechanism (Fig. 1a) is attached to the subject elbow joint, and the driving torque generated by the geared motor (Fig. 1b) is transmitted to the joint side through a Bowden cable to affect the joint side motion. The torsional spring between the motor side and the joint side acts as an energy buffer and a torque sensor.

A. Selection of Geared Motor

A DC motor is used to provide the actuation to the system. In order to realize zero output torque control of the cable-driven RSEA for motion tracking, the motor should be selected based on the characteristics of the subject motion, among which joint torque and speed are the major factors. The actuator proposed in this paper is designed for motion tracking of a macaque elbow joint. Fig. 2 shows a typical elbow kinematic motion of a macaque during a 3-dimensional reach-grasp-self-feed movement to a food target. It can be seen that the typical peak speed during the designed task is about 2.6rad/s, which matches the result of the reach-grasp movement in [9] well. In addition, the maximum elbow speed of a macaque performing the reach-grasp movement found in [9] is 7.8rad/s. Measuring the joint torques of an animal

[1]J. Lu, K. Haninger, and M. Tomizuka are with the Department of Mechanical Engineering, University of California, Berkeley, CA 94720 USA e-mail: {junkai.lu, khaninger, tomizuka}@berkeley.edu

[2]W. Chen is with the FANUC Corporation, Oshino-mura, Yamanashi Prefecture 401-0597, Japan e-mail: wjchen@berkeley.edu
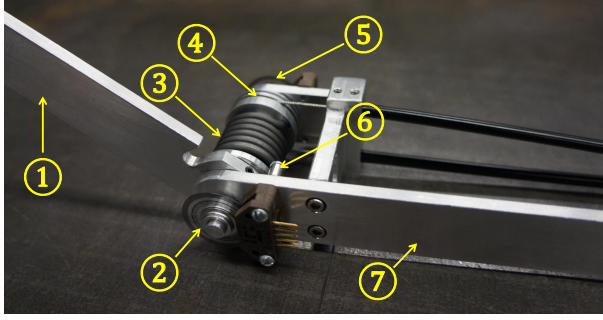
(a) Joint side design consisting of: ① moving linkage, ② subject-side encoder (1250 counts/round), ③ spring, ④ joint-side pulley, ⑤ joint-side encoder (1250 counts/round), ⑥ mechanical stop, ⑦ fixed linkage.
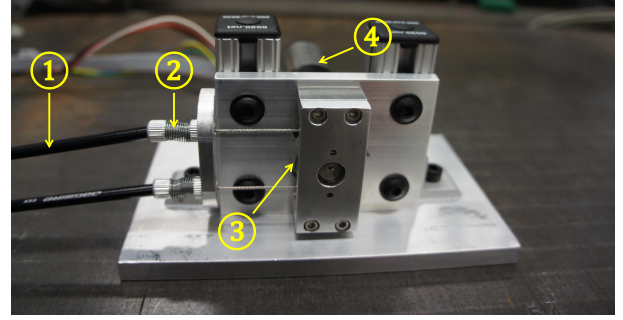
(b) Motor side design consisting of: ① Bowden cable, ② barrel adjuster, ③ gearbox pulley, ④ geared motor with optical encoder (1000 counts/round).

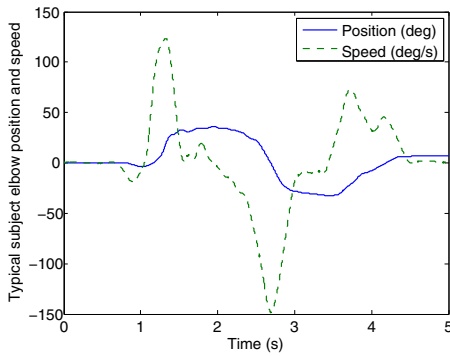Fig. 1. Hardware setup of the proposed cable-driven RSEA.

Fig. 2. Typical elbow kinematic motion of the subject during 3D reach-grasp-self-feed movement to a target[1]. Motion data was collected by the passive macaque exoskeleton presented in [12] .

is complicated and time-consuming, thus literature on the estimate of macaque joint torques are used. [10] shows that the typical elbow joint torque of a macaque during a "center-out" task is 0.2Nm, and [11] indicates that the peak muscle torque of the macaque elbow joint can be as large as 9.4Nm.

Generally joint torques at high speed should be relatively small, thus an elbow joint torque of 1.0Nm at a maximum speed of 7.0rad/s is assumed for the macaque subject in the current design, which results in a maximum power of 7.0W. A 30% power transmission efficiency is also assumed considering the efficiency of the motor (70%), the gearbox (70%) and the transmission efficiency of force by the Bowden cable (assumed to be 60% due to friction loss). Thus the rated motor power should be larger than 24W. Considering the safety factor of two [4], a Maxon EC-max 30 brushless DC motor with a nominal power of 40W is selected, which has a nominal speed of 7220r/min, a maximum continuous torque of 0.0338Nm and a stall torque of 0.16Nm. To provide sufficient torques in the proper range of speed, a

Maxon planetary gearbox with a speed reduction ratio of 132:1 is selected. Thus the nominal output speed, maximum continuous torque and stall torque of the geared motor are about 5.7rad/s, 4.5Nm and 21Nm, respectively, which will be sufficient for the current application.

B. Selection of Torsional Spring

The elastic element plays an important role in the SEA design. On one hand, it introduces the compliance in the actuation mechanism, which can accommodate the low in-trinsic stiffness of the subject body and thus ensure the safety during subject-robot interaction; on the other hand, it serves as a torque sensor which can save the space and cost of a dedicated one. The considerations on interaction safety and torque resolution require a more compliant elastic component in the SEA. However, compliant elasticity in the elastic component cannot provide sufficiently large output force/torque, and also may reduce the large force bandwidth of the SEA [13]. Therefore, a balance should be made among all these factors. So far a heuristic way of selecting the elasticity of the elastic component for an SEA is utilized with tests of springs with different stiffnesses.

Per the above discussions, a collection of torsional springs with the stiffness of 3.49, 7.61, 16.43 and 27.03Nm/rad were examined, and in the end we chose the first one to be implemented for the zero output torque control work presented in this paper.

C. Selection of Power Transmission

To achieve a compact and lightweight actuator design, a cable-driven mechanism which avoids attaching the motor to the subject is used in the proposed design. The motor is installed on a stationary base and the driving force from the motor is transmitted through the cables to the subject joint. The Bowden cable, which is difficult to extend but easy to wind, is selected for our application. To reduce backlash, a pair of barrel adjusters are used for adjusting the preload cable tension. One big challenge of introducing the Bowden cable is to deal with the variable friction between its tendon and sheath [6], and this will be detailed in Section III-B.

[1]One adult male rhesus macaque was used in this study. All procedures were conducted in compliance with the National Institute of Health Guide for Care and Use of Laboratory Animals and were approved by the University of California, Berkeley Institutional Animal Care and Use Committee.

Fig. 3. Schematic representation of the actuator-subject system.

Fig. 4. Block diagram of the actuator-subject system.

Fig. 5. Equivalent open loop model of the torque-mode control system.

III. SYSTEM MODELING AND CONTROL

A. System Modeling

Fig. 3 shows a schematic of the actuator-subject system labeled with key kinematic and kinetic quantities. The equations of motion of the system are

$$J_m\ddot{\theta}_m + \tau_{fr,m} + \tau_{fr,gm} = u - \tau_{\text{in},g}, \qquad (1)$$

$$J_g\ddot{\theta}_g + \tau_{fr,gb} + \tau_\ell = \tau_{\text{out},g}, \qquad (2)$$

$$\tau_{\text{out},g} = N \cdot \tau_{\text{in},g}, \qquad (3)$$

$$\theta_m = N \cdot \theta_g, \qquad (4)$$

$$\tau_\ell = \tau_{fr,\text{cable}} + \tau_o + \tau_{fr,jpb}, \qquad (5)$$

$$\tau_o = k_{\text{spring}}(\theta_{jp} - \theta_s), \qquad (6)$$

$$\tau_s + \tau_o = J_s\ddot{\theta}_s + \tau_{fr,jsb} + \tau_{\text{grav}}, \qquad (7)$$

$$\theta_{jp} = \frac{r_{gp}}{r_{jp}}\theta_g. \qquad (8)$$

where J_m, J_g and J_s are the inertia of the motor, the gearbox and the subject body segment, respectively; $\tau_{fr,m}$, $\tau_{fr,gm}$, $\tau_{fr,gb}$, $\tau_{fr,jpb}$, $\tau_{fr,jsb}$, and $\tau_{fr,\text{cable}}$ are the friction torque of the motor, the gear meshing, the bearing on the gearbox side, the bearing on the joint-pulley side, the bearing on the subject joint side, and the Bowden cable, respectively; $\tau_{\text{in},g}$ and $\tau_{\text{out},g}$ are the gearbox input and output torque, respectively; τ_o, τ_s, τ_ℓ and τ_{grav} are the actuator output torque, the subject joint torque, the load torque and the torque due to the gravity force of the subject's body, respectively; θ_m, θ_g, θ_{jp} and θ_s are the angular displacement of the motor, the gearbox, the joint side pulley and the subject joint, respectively; u is the input torque command to the motor, N is the gearbox reduction ratio, k_{spring} is the spring stiffness coefficient; r_{jp} and r_{gp} are the radius of the joint-side pulley and the gearbox pulley, respectively.

Eq. (1) $\sim$ (4) yield

$$J_M\ddot{\theta}_m + \tau_{fr,M} = u - \frac{1}{N}\tau_\ell, \qquad (9)$$

where $J_M := J_m + J_g/N^2$ and $\tau_{fr,M} := \tau_{fr,gb}/N + \tau_{fr,m} + \tau_{fr,gm}$ represent the equivalent inertia of the geared motor and the equivalent friction torque referred to the motor side, respectively. Considering the feasibility of implementation, it is reasonable to group several friction torques together as an equivalent one reflected on the motor side for modeling and estimation [14]. To characterize the friction torque, the following model is used [15]

$$\tau_{fr,M} = \beta_M\dot{\theta}_m + \tau_{fr,M}^{nl}, \qquad (10)$$

where β_M is the damping coefficient with respect to the motor speed $\dot{\theta}_m$, and $\tau_{fr,M}^{nl}$ includes all the nonlinear friction.

Fig. 4 shows the block diagram of the actuator-subject system. u is the driving force of the motor loop (denoted as L_1), and the resultant torque $\tau_s' := \tau_s - \tau_{fr,jsb} - \tau_{\text{grav}}$ is the driving force of the subject loop (denoted as L_2); the two loops are connected by the torsional spring. $\tau_{fr,M}^{nl}$ and $\tau_{fr,\text{cable}} + \tau_{fr,jpb}$ can be regarded as the disturbances to the system, which should be rejected by the controllers. The output of the system is τ_o when the system is running in a torque control mode, and θ_s when running in a position control mode, respectively. We will only focus on the torque control, specifically zero output torque control, in this paper.

B. Controller Design

1) DOB Based Torque-Mode Controller Design: In the torque-mode control of RSEAs, the goal is to control the output torque $\tau_o = k_{\text{spring}}(\theta_{jp} - \theta_s)$ to the desired value, and in turn, with such assistive torque, the subject can adjust his/her joint torque τ_s accordingly to generate the desired joint motion θ_s. However, the subject body segment inertia J_s and the resultant torque τ_s' applied by the subject are unknown. Thus θ_s can be regarded as a "disturbance" to the system [3], [16], which is measurable due to the encoder mounted on the subject joint side. Therefore, the L_2 loop in Fig. 4 can be regarded as cut open, and θ_s can be treated as a known exogenous reference to the system. A discrete-time equivalence of such system is shown in Fig. 5, where $d := -\tau_{fr,M}^{nl} - (\tau_{fr,\text{cable}} + \tau_{fr,jpb})/N$ is the equivalent disturbance, $\tilde{\tau}$ is a fictitious output torque, $G(z^{-1}) := Nk_{\text{spring}}P(z^{-1})/(k_{\text{spring}}P(z^{-1}) + N)$, $G_s(z^{-1}) := Nk_{\text{spring}}/(k_{\text{spring}}P(z^{-1}) + N)$, and $P(z^{-1})$ is the zero-order hold (ZOH) equivalence of the geared motor model $P(s) := \frac{1}{s(J_Ms + \beta_M)} \cdot \frac{r_{gp}}{Nr_{jp}}$.

Since the friction on the Bowden cable is sheath profile dependent [6], [17], and the cable is mobile in practical applications, the rejection of such variable friction is a challenge to achieve perfect torque control of the cable-driven RSEA. The DOB has the advantage of robust disturbance rejection and the ability of shaping the actual plant to the nominal plant model at specific frequency range, thus a DOB based control algorithm is proposed in this work.

Fig. 6 shows the block diagram of the proposed DOB based torque-mode control system with τ_d being the desired output torque. The nominal plant model to be controlled is defined as follows

$$G_n(z^{-1}) = \frac{N k_{\text{spring}} P_n(z^{-1})}{k_{\text{spring}} P_n(z^{-1}) + N} := z^{-m_n} \bar{G}_n(z^{-1}), \quad (11)$$

where $P_n(z^{-1})$ is the nominal model of the geared motor, $Q(z^{-1})$ is a low-pass filter to be designed. m_n is the number of pure delay steps, and $\bar{G}_n(z^{-1})$ is the remaining dynamics without any pure delay; the separation of m_n and $\bar{G}_n(z^{-1})$ is required by a discrete-time version of DOB to make the DOB loop causal. $\bar{G}_n(z^{-1})$ is directly invertible if it is stable and minimum phase.

We now have

$$G_{\tilde{u}\tilde{\tau}}(z^{-1}) = \frac{G \bar{G}_n}{\bar{G}_n + Q(z^{-1}) \left(G - z^{-m_n} \bar{G}_n \right)}, \quad (12)$$

$$G_{d\tilde{\tau}}(z^{-1}) = \frac{G \bar{G}_n \left(1 - Q(z^{-1}) z^{-m_n} \right)}{\bar{G}_n + Q(z^{-1}) \left(G - z^{-m_n} \bar{G}_n \right)}. \quad (13)$$

In the low frequency region where $Q(z^{-1}) \approx 1$, if the delay is sufficiently small such that $(1 - z^{-m_n}) \bar{G}_n(z^{-1}) \approx 0$, then $G_{\tilde{u}\tilde{\tau}}(z^{-1}) \approx G_n(z^{-1})$ and $G_{d\tilde{\tau}}(z^{-1}) \approx 0$ [18], which indicates that the DOB makes the dynamics from $\tilde{u}$ to $\tilde{\tau}$ behave like the nominal plant and rejects low frequency disturbances. The DOB loop was then stabilized by an outer controller $C(z^{-1})$ to meet the performance requirements.

2) Stability of the DOB Loop: To investigate the stability robustness of the DOB loop, assume that there is a multiplicative uncertainty $\Delta(z^{-1})$ between the actual and the nominal equivalent plant

$$G(z^{-1}) = G_n(z^{-1}) \left(1 + \Delta(z^{-1}) \right). \quad (14)$$

By small gain theorem, the DOB loop will be stable if [8]

$$\left\| \Delta(e^{j\omega}) Q(e^{j\omega}) \right\|_\infty < 1, \text{ for } \forall \omega \in [0, \pi). \quad (15)$$

3) Stability of the Overall Actuator-Subject System: For the stability of this overall system (loop L_1 plus loop L_2 as shown in Fig. 4), consider the equilibrium point where the subject is stationary under the influence of gravity, joint side bearing friction, and subject's own voluntary torque, i.e., $\tau_s' = 0$. Then the perturbation of θ_s will be subject to the actual output torque τ_o. In this case, the L_2 loop should be closed with L_1, and the assumption that θ_s acts as an independent motion disturbance to the L_1 loop will not hold. Thus analyzing the stability of the overall actuator-subject system is important to guarantee the subject safety.

Assume that the DOB works perfectly in the low frequency region, the block diagram of the combined actuator-subject system can be reduced as shown in Fig. 7 with $P_s(z^{-1})$ being the ZOH equivalence of $P_s(s) := 1/(J_s s^2)$; the subject body segment inertia J_s is not well known. To guarantee the stability of the overall actuator-subject system, the closed loop system in Fig. 7 should be stable.

The stability criteria derived above will provide a guidance for the practical controller design and stability analysis as shown in the next section.

IV. IMPLEMENTATION AND EXPERIMENTAL RESULTS

A. System Identification

The DOB based controller design technique is generally regarded as an identification-free approach, and thus the inertia and damping of the geared motor may be assigned using the nominal values on datasheets, or even arbitrarily selected [19]. However, system identification is still necessary for designing the Q-filter and the controller $C(z^{-1})$, as well as analyzing the stability of the overall system.

1) Identification of the Damping of the Geared Motor: We know from (10) that the damping of a geared motor can be included in the equivalent friction torque $\tau_{fr,M}$, and thus the identification of β_M is turned into a problem of friction torque identification of the geared motor. (9) shows that $\tau_{fr,M}$ will exactly be equal to the input torque command of the motor u if the unloaded geared motor is running in a constant speed control mode. Fig. 8 plots the experimentally measured friction torques at different motor side speeds which perfectly matches the static friction model with the Stribeck effect [20] as follows

$$\tau_{fr,M} = \sigma \dot{\theta}_m + \left(\tau_{CL} + (\tau_{st} - \tau_{CL}) e^{-(\dot{\theta}_m/\dot{\theta}_{SB})^2} \right) \text{sgn}(\dot{\theta}_m), \quad (16)$$

where σ, τ_{CL}, τ_{st} and $\dot{\theta}_{SB}$ represent the damping coefficient, the Coulomb friction, the static friction and the Stribeck speed, respectively.

By applying a nonlinear least squares fitting, the identified parameters are $\sigma = 8.022 \times 10^{-7}$Nm·sec/rad, $\tau_{CL} = 2.384 \times 10^{-3}$Nm, $\tau_{st} = 1.425 \times 10^{-3}$Nm, $\dot{\theta}_{SB} = 130.75$rad/sec. This friction model cannot be directly used for friction compensation since this approach is not able to satisfactorily identify τ_{st} and $\dot{\theta}_{SB}$; however, the estimation of σ is generally of high quality [14], [20]. This is also why the nonlinear friction term is treated as a disturbance and the DOB is used to reject such friction as discussed in previous sections.

We may directly assign the damping of the geared motor β_M to be equal to σ as identified above. However, when taking a close look at Fig. 8 we notice that σ matches the geared motor damping in the high speed region (> 200rad/s) well rather than that in the low speed region (< 200rad/s). In this case, one natural way would be gain scheduling, which adjusts the damping coefficient in the nominal model according to the speed region. This however introduces the controller complexity and stability issue during parameter switching. Alternatively, we could use a uniform damping value as a trade-off between the low and high speed regions, although model mismatch would occur accordingly. Further
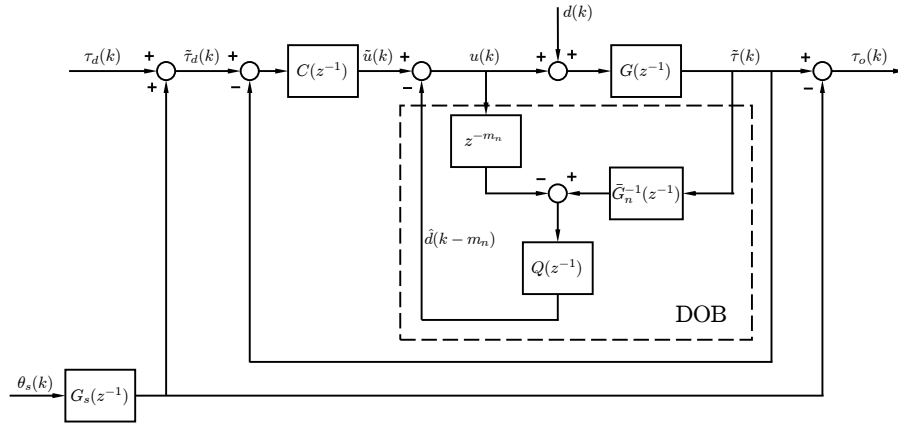
Fig. 6. Block diagram of the DOB based torque-mode control system.
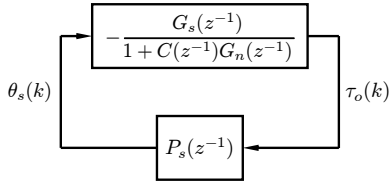

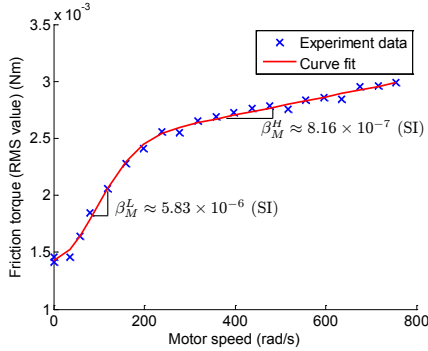Fig. 7. Block diagram of the simplified actuator-subject system with DOB.

Step input level ($\times 10^{-3}$Nm)	J_M (kg·m^2)	β_M (Nm·sec/rad)
$1.22 \to 1.94$	1.85×10^{-6}	5.50×10^{-6}
$1.22 \to 2.19$	1.86×10^{-6}	5.31×10^{-6}
$1.22 \to 2.43$	1.85×10^{-6}	5.53×10^{-6}

Fig. 8. Steady-state speed-friction characteristic of the geared motor.

discussions about the selection of damping will be detailed in Section IV-B.2.

2) Identification of the Inertia of the Geared Motor:
The inertia of the geared motor J_M is identified by investigating the step responses from the input torque u to the unloaded motor side speed $\dot{\theta}_m$. To overcome the static friction τ_{st}, the step responses were collected by starting at $u = 1.22 \times 10^{-3}$Nm and ending at 1.94×10^{-3}, 2.19×10^{-3}, 2.43×10^{-3}Nm, respectively. Then J_M was identified by estimating the transfer function $1/(J_M s + \beta_M)$ using the `tfest` function in MATLAB [21].

Table I shows the identified inertia and damping of the geared motor with different step input levels. It turns out that the identified inertia values are quite consistent. Since the step input levels are selected to generate a steady-state speed in the low motor speed region, the identified dampings

match Fig. 8 well.

B. Controller Design and Stability Analysis

1) Design of $C(z^{-1})$: Generally the outer controller $C(z^{-1})$ is designed before the Q-filter based on the nominal model $G_n(z^{-1})$. In this work the $C(z^{-1})$ is selected as a PID controller. To ensure the requirements of robust stability and bandwidth, the PID gains are set to be $K_P = 0.716$, $K_I = 2.073$ and $K_D = 0.0085$. The controller is digitally implemented using the LabVIEW Real-Time Operating System (National Instrument) with a sampling rate of 1kHz.

2) Design of Q-filter: The low-pass filter $Q(z^{-1})$ is selected to be a third-order binomial filter [22], and then discretized using the bilinear transform

$$Q(z^{-1}) = \frac{3(\tau s) + 1}{(\tau s)^3 + 3(\tau s)^2 + 3(\tau s) + 1}\Big|_{s = \frac{2}{T}\frac{z-1}{z+1}}, \quad (17)$$

where T is the sampling period, and $\tau = 2\pi/w_c$ with ω_c being the desired cutoff frequency of the Q-filter.

To guarantee the stability of the DOB loop, it is required by (15) that the magnitude of the Q-filter should always be smaller than that of the inverse of the multiplicative uncertainty. In this work we assume that the only source of uncertainty is introduced by the difference of the damping value β_M in the low motor speed region and in the high speed region, as is discussed in Section IV-A.1.

Fig. 9a shows the relationship between $||Q(e^{j\omega})||$ and $||\Delta^{-1}(e^{j\omega})||$ in the case of directly using either β_M^L or β_M^H. We notice that when $\beta_M = \beta_M^L$, the resulting $\Delta_1^{-1}(e^{j\omega})$ due to β_M^H already crosses the Q-filter curve; if we assign $\beta_M = \beta_M^H$, the resulting $\Delta_2^{-1}(e^{j\omega})$ almost overlaps with the Q-filter as well. Then a compromised value is selected as $\beta_M = 1.37 \times 10^{-6}$ (SI), and the relationship between
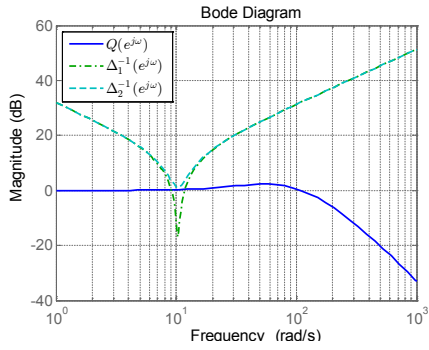
(a) Using either β_M^L or β_M^H
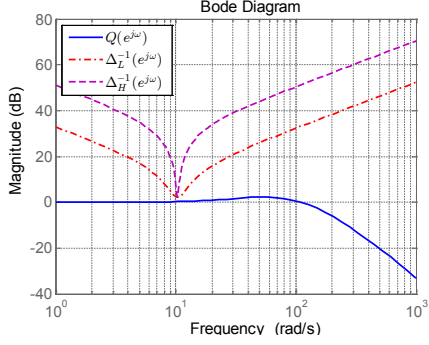
(b) Using a compromised β_M

Fig. 9. Selection of β_M for the Q-filter (cutoff frequency 15Hz) design.
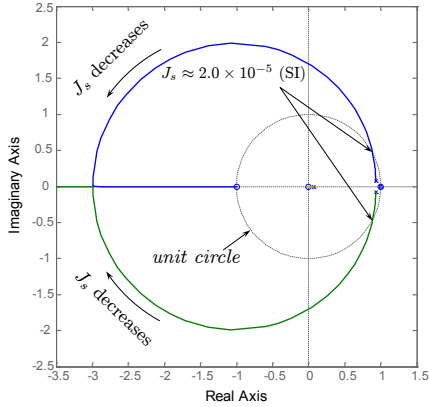

Fig. 10. Root locus of the closed loop actuator-subject system.

$||Q(e^{j\omega})||$ and $||\Delta^{-1}(e^{j\omega})||$ is shown in Fig. 9b, from which we can see that the stability condition is satisfied.

3) Stability of the Overall System: Now that the equivalent plant model $G_n(z^{-1})$ and the controller $C(z^{-1})$ have been specified, the stability of the overall actuator-subject system can be investigated by studying the poles of the closed loop system shown in Fig. 7. Fig. 10 plots the root locus of this closed loop system as a function of the subject body segment inertia J_s. As long as J_s is larger than the critical value 2.0×10^{-5} kg·m^2, the overall closed loop system would be stable. Based on the approach proposed in [23], the estimated J_s for the three male macaques in the BMI study are 3.2×10^{-3}, 4.1×10^{-3} and 3.3×10^{-3} kg·m^2,
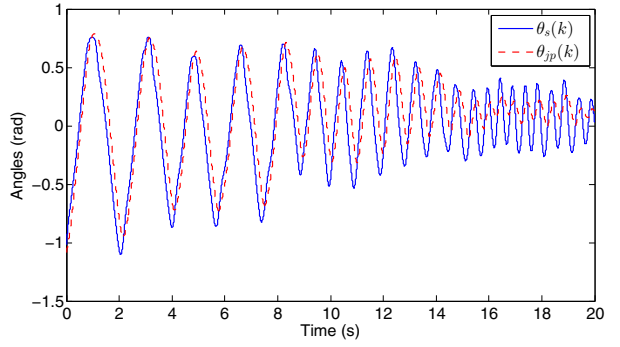
(a) Plots of θ_s and θ_{jp} for different subject motion frequencies.
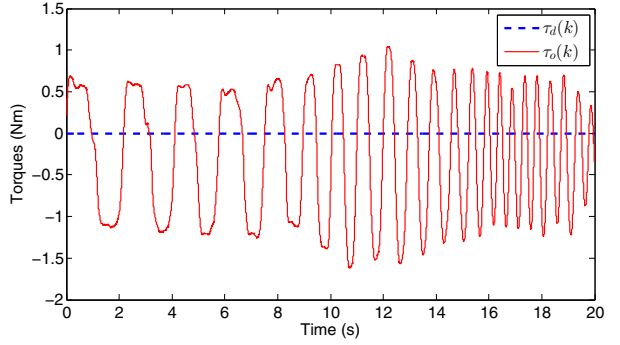
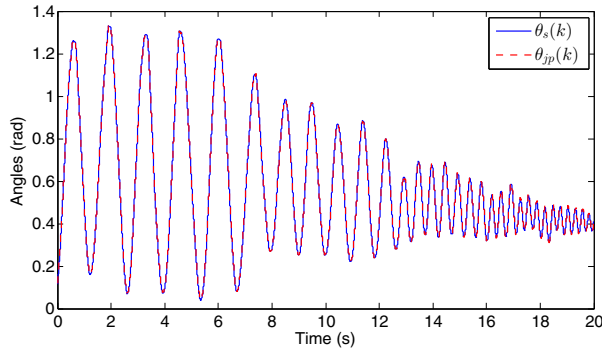(b) Plots of the desired torque and the actual output torques.

Fig. 11. Experiment results with no control.

respectively. Thus the overall actuator-subject system can be regarded as stable.

C. Experiment Verification with a Human Subject

Since conducting experiments directly with the macaques is not feasible at current stage, some preliminary experiments were completed with a human subject. During the experiments, the desired output torque τ_d was set to be identically zero, and the human subject was instructed to rotate the moving linkage (① in Fig. 1a) with different frequencies of motion. Fig.11 presents the experimental results when no control was applied to the actuator. It can be seen that the joint-side pulley (④ in Fig. 1a) which is connected to the motor could hardly follow the subject motion. The actuator exhibited very low backdrivability due to the amplified friction of the geared motor by the high greabox reduction ratio, and the resistive spring torques were significant.

Fig. 12 shows the experimental results of one trial when the proposed torque-mode control algorithm was applied. It can be seen from Fig. 12a that the actuator managed to follow the subject motion to keep the spring deflection small in a wide range of frequencies. The subject reported that he could feel slight vibrations during the experiment, but the magnitude of the resistive torques were very small, as reflected in Fig. 12b. The maximum absolute output torque error was within 0.05Nm, and the root-mean-square (RMS) error was about 0.0096Nm, which indicates the effectiveness of the proposed design.

(a) Plots of θ_s and θ_{jp} for different subject motion frequencies.
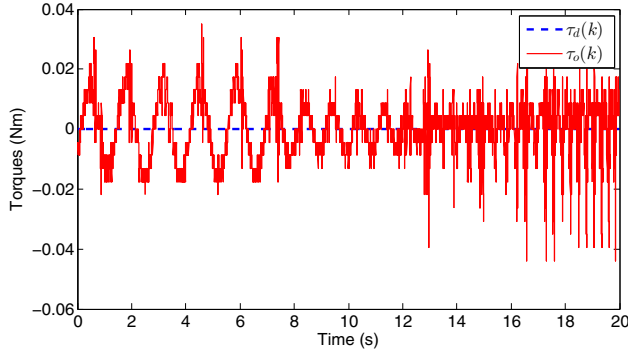
(b) Plots of the desired torque and the actual output torques.

Fig. 12. Experiment results with torque-mode control algorithm.

V. CONCLUSIONS AND FUTURE WORK

This paper presented a design of a cable-driven RSEA for zero output torque control during the subject-robot interaction. The mechanical design was first described in terms of hardware selection. To achieve zero output torque control of the proposed actuator in the presence of variable friction of the Bowden cable, the considerations of choosing the damping and inertia parameters of the geared motor were discussed, and the DOB based torque-mode control algorithm was developed. Stabilities of the DOB loop and the overall subject-robot system were then carefully analyzed. The performance of the proposed design was supported by the experiments with a human subject.

Future work will focus on the effect of different cable profiles on the control algorithm performance, as well as the development of position control and impedance control strategies of the cable-driven RSEA for next step research goals in the BMI study.

ACKNOWLEDGMENT

REFERENCES

[1] G. A. Pratt and M. M. Williamson, "Series elastic actuators," in *Proc. IEEE/RSJ Int. Conf. Intell. Robots Syst. (IROS)*, vol. 1, Aug 1995, pp. 399–406.

[2] K. Kong, J. Bae, and M. Tomizuka, "Control of rotary series elastic actuator for ideal force-mode actuation in human-robot interaction applications," *IEEE/ASME Trans. Mechatronics*, vol. 14, no. 1, pp. 105–118, Feb 2009.

[3] D. Ragonesi, S. Agrawal, W. Sample, and T. Rahman, "Series elastic actuator control of a powered exoskeleton," in *Proc. 33rd Annu. IEEE Int. Conf. on Eng. in Med. and Biol. Soc. (EMBC)*, Aug 2011, pp. 3515–3518.

[4] K. Kong, J. Bae, and M. Tomizuka, "A compact rotary series elastic actuator for human assistive systems," *IEEE/ASME Trans. Mechatronics*, vol. 17, no. 2, pp. 288–297, April 2012.

[5] W. dos Santos, G. Caurin, and A. Siqueira, "Torque control characterization of a rotary series elastic actuator for knee rehabilitation," in *Proc. 16th Int. Conf. Adv. Robotics (ICAR)*, Nov 2013, pp. 1–6.

[6] K. Kong, J. Bae, and M. Tomizuka, "Torque mode control of a cable-driven actuating system by sensor fusion," *J. Dyn. Sys., Meas., Control*, vol. 135, no. 3, pp. 031 003–1 − 031 003–7, May 2013.

[7] K. Ohnishi, M. Shibata, and T. Murakami, "Motion control for advanced mechatronics," *IEEE/ASME Trans. Mechatronics*, vol. 1, no. 1, pp. 56–67, March 1996.

[8] C. Kempf and S. Kobayashi, "Disturbance observer and feedforward design for a high-speed direct-drive positioning table," *IEEE Trans. Control Syst. Technol.*, vol. 7, no. 5, pp. 513–526, Sep 1999.

[9] M. I. Christel and A. Billard, "Comparison between macaques' and humans' kinematics of prehension: the role of morphological differences and control mechanisms," *Behav. Brain Res.*, vol. 131, no. 1-2, pp. 169–184, 2002.

[10] S. S. Chan and D. W. Moran, "Computational model of a primate arm: from hand position to joint angles, joint torques and muscle forces," *J. Neural Eng.*, vol. 3, no. 4, pp. 327–337, 2006.

[11] K. M. Graham and S. H. Scott, "Morphometry of macaca mulatta forelimb. III. moment arm of shoulder and elbow muscles," *J. Morphol.*, vol. 255, no. 3, pp. 301–314, 2003.

[12] J. Lu, W. Chen, K. Haninger, and M. Tomizuka, "A passive upper limb exoskeleton for macaques in a BMI study – kinematic design, analysis, and calibration," in *Proc. ASME Dyn. Syst. Control Conf. (DSCC)*, 2014, pp. V003T43A001–V003T43A009.

[13] D. W. Robinson, "Design and analysis of series elasticity in closed-loop actuator force control," Ph.D. dissertation, Massachusetts Institute of Technology, Cambridge, MA, 2000.

[14] W. Chen, K. Kong, and M. Tomizuka, "Dual-stage adaptive friction compensation for precise load side position tracking of indirect drive mechanisms," *IEEE Trans. Control Syst. Technol.*, vol. 23, no. 1, pp. 164–175, 2015.

[15] B. Armstrong-Helouvry, P. Dupont, and C. Canudas de Wit, "A survey of models, analysis tools and compensation methods for the control of machines with friction," *Automatica*, vol. 30, no. 7, pp. 1083–1138, 1994.

[16] M. Grun, R. Muller, and U. Konigorski, "Model based control of series elastic actuators," in *Proc. IEEE/RAS-EMBS Int. Conf. on Biomed. Robot. Biomechatronics (BioRob)*, June 2012, pp. 538–543.

[17] M. Kaneko, T. Yamashita, and K. Tanie, "Basic considerations on transmission characteristics for tendon drive robots," in *Proc. 5th Int. Conf. Adv. Robotics (ICAR)*, vol. 1, June 1991, pp. 827–832.

[18] X. Chen and M. Tomizuka, "Optimal plant shaping for high bandwidth disturbance rejection in discrete disturbance observers," in *Proc. Amer. Cont. Conf. (ACC)*, June 2010, pp. 2641–2646.

[19] M. J. Kim and W. K. Chung, "Robust control of flexible joint robots based on motor-side dynamics reshaping using disturbance observer (DOB)," in *Proc. IEEE/RSJ Int. Conf. Intell. Robots Syst. (IROS)*, 2014, pp. 2381–2388.

[20] F. Altpeter, "Friction modeling, identification and compensation," Ph.D. dissertation, Ecole Polytechnique Federale de Lausanne, Lausanne, Switzerland, 1999.

[21] MathWorks. (2014) System Identification Toolbox. [Online]. Available: http://www.mathworks.com/products/sysid/

[22] H. S. Lee and M. Tomizuka, "Robust motion controller design for high-accuracy positioning systems," *IEEE Trans. Ind. Electron.*, vol. 43, no. 1, pp. 48–55, Feb 1996.

[23] J. A. Vilensky, "Masses, centers-of-gravity, and moments-of-inertia of the body segments of the rhesus monkey (macaca mulatta)," *AM. J. PHYS. ANTHROP.*, vol. 50, pp. 57–66, 1979.